Material properties from acoustic radiation force step response

Marko Orescanin
Department of Electrical and Computer Engineering, University of Illinois at Urbana-Champaign, Urbana, Illinois 61801

Kathleen S. Toohey
Department of Bioengineering, University of Illinois at Urbana-Champaign, Urbana, Illinois 61801

Michael F. Insana
Department of Bioengineering, Department of Electrical and Computer Engineering, Beckman Institute for Advanced Science and Technology, University of Illinois at Urbana-Champaign, Urbana, Illinois 61801

An ultrasonic technique for estimating viscoelastic properties of hydrogels, including engineered biological tissues, is being developed. An acoustic radiation force is applied to deform the gel locally while Doppler pulses track the induced movement. The system efficiently couples radiation force to the medium through an embedded scattering sphere. A single-element, spherically-focused, circular piston element transmits a continuous-wave burst to suddenly apply and remove a radiation force to the sphere. Simultaneously, a linear array and spectral Doppler technique are applied to track the position of the sphere over time. The complex shear modulus of the gel was estimated by applying a harmonic oscillator model to measurements of time-varying sphere displacement. Assuming that the stress-strain response of the surrounding gel is linear, this model yields an impulse response function for the gel system that may be used to estimate material properties for other load functions. The method is designed to explore the force-frequency landscape of cell-matrix viscoelasticity. Reported measurements of the shear modulus of gelatin gels at two concentrations are in close agreement with independent rheometer measurements of the same gels. Accurate modulus measurements require that the rate of Doppler-pulse transmission be matched to a priori estimates of gel properties. © *2009 Acoustical Society of America.* [DOI: 10.1121/1.3106129]

I. INTRODUCTION

Elasticity imaging is a promising diagnostic technique for discriminating between benign and malignant breast lesions.[1–7] Its diagnostic value stems from the important role of the cellular mechanoenvironment in regulating tumor growth[8] and from the large tumor contrast observed for various mechanical properties.[9] Biological sources of elastic strain contrast in mammary tissues include edema, hyperplasia, acidosis, fibrosis, desmoplasia, and inflammatory responses characteristic of the reaction of breast stroma to cancer cells. Physical sources of elasticity contrast are related to the spatial variations in flow velocity of fluids through the extracellular matrix (poroelasticity) and the rate at which the matrix itself mechanically relaxes (viscoelastic) in response to applied forces.[10] Classification of nonpalpable, isoelastic lesions is possible by imaging time-varying strain features.[6,7]

Despite early clinical successes, the visibility of lesions in elasticity imaging can vary widely. We hypothesize that some of the clinical variability may be reduced by improving our understanding of elasticity imaging contrast mechanisms and adapting the imaging techniques accordingly. Our approach to mechanism discovery is to establish relationships between the physical and biological sources of contrast listed above across the spectrum of force frequencies used by the various approaches to elasticity imaging.

Quasi-static elasticity imaging methods apply a ramp force suddenly and hold it constant while strain is imaged over time.[11] The methods is "quasi-static" for patient imaging because modest forces (1–5 N) are manually applied slowly (~1-s ramp on) to the breast surface through the ultrasound transducer. Quasi-static methods interrogate tissues at a very low applied-load frequency bandwidth that is bounded from above at approximately 1 Hz and from below at 0.01 Hz depending on the total acquisition time for the strain image recording sequence.[12] At the other load bandwidth extreme are acoustic radiation force imaging methods.[5] A focused push-pulse applies a weak impulse force deep in tissue for about 1 ms after which displacements are imaged in time as the tissue relaxes. This load bandwidth is nominally 100–1000 Hz depending on experimental details. Other acoustic-based approaches, including ultrasound-stimulated vibro-acoustic spectography,[2] shear wave elasticity imaging,[3] and harmonic motion imaging,[4] probe load bandwidths somewhere between these two extremes.

It is difficult to design studies to discover disease-specific sources of elasticity contrast for any of these imaging techniques. *In vivo* breast tissue properties are spatially heterogeneous, frequently anisotropic, and have poorly defined boundaries. Hence complex internal stress fields are common, making it difficult to even rigorously define a modulus. Excised tissue samples are nonrepresentative be-

cause of changes caused by the lack of perfusion, decomposition, or use of fixatives. Gelatin hydrogels are structurally simpler, homogeneous, and able to mimic some properties of breast stroma as required for imaging system development.[12] However, hydrogels do not mimic cell-driven dynamic properties normally associated with malignant progression or responses to treatment; many of these features are assumed associated with tumor contrast. Rodent models of mammary cancer can accurately represent genomic, biochemical, metabolic, and some perfusion aspects of tumor physiology,[13] but are less representative of the macrostructures of human breast tumors that strongly influence mechanical behavior.

We are exploring the use of three dimensional (3D) cell cultures.[14,15] While they suffer many of the same problems experienced in excised tissue measurements, they have the advantage of containing living mammary cells embedded in hydrogel volumes. The cells can be biochemically or mechanically stimulated and then observed under sterile conditions. Cell cultures do not simulate the tumor macroanatomy but they can mimic the responses of tumor-cell clusters to their microenvironment. Gels combine geometric simplicity for ease of mechanical measurements with dynamic cellular processes that can be independently verified via optical microscopy.

Many biological tissues and all of the gels we considered are biphasic polymers, which means their mechanical properties are determined by a polymeric matrix (solid phase) embedded in a liquid (fluid phase). The mechanical responses of multiphasic polymers depend significantly on the rate at which force is applied. For example, the complex shear modulus is known to vary widely with force frequency in lightly-cross-linked amorphous polymers,[16] breast tissues,[6] and even within individual cells of the body.[17]

Our research goal is to develop a radiation force technique for estimating shear modulus and shear viscosity of gel types often used in 3D cell cultures and engineered tissues. These measurements will eventually be made over the bandwidth of force frequencies used in various elasticity imaging techniques. This report focuses on the application of Doppler measurements to describe transient dynamic responses of gelatin gels to a step change in radiation force. Particle velocity estimates are related to modulus and viscosity through a second-order rheological model. The results provide an estimate of the impulse response function of shear wave imaging.

II. METHODS

The goal of the proposed method is to remotely and quantitatively estimate material properties using acoustic radiation force. Acoustic pressure fields exert localized forces with a magnitude that depends on the energy density of the field and the scattering and absorption properties of target media. Gelatin gels are used in this study that describes the measurement system and rheological models applied for material property estimation.
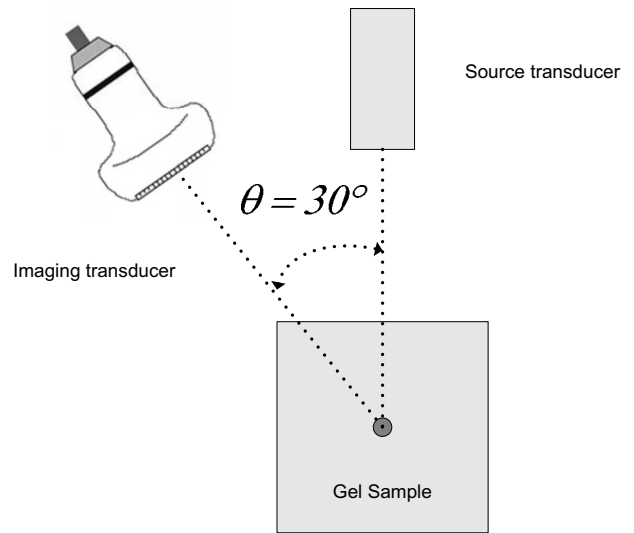
FIG. 1. Diagram of the experiment to measure viscoelastic properties of gel samples. Acoustic force applied by a source transducer displaces a sphere embedded in the gel. An imaging transducer tracks the induced motion of the sphere.

A. Acoustic radiation force

Acoustic radiation force is generated when momentum of the acoustic wave is transferred to the propagation medium via attenuation and scattering interactions. We study low-attenuation gels to which a strongly scattering sphere is embedded. Scattering from the sphere efficiently couples the acoustic field to the gel to induce forces that measurably deform gels at relatively low acoustic intensity.

For sphere diameters small compared with the beam width (1.5 and 6 mm, respectively), we can assume local plane waves and the time-averaged force on the scattering sphere is approximately[18]

$$F = \pi a^2 Y \bar{E}. \tag{1}$$

The quantity a is the sphere radius and Y is the radiation force function as determined by the mechanical properties and geometry of the sphere and the surrounding gel. $\bar{E}$ is the average energy density of the incident field. The time average is over several cycles of the carrier frequency (microseconds) but typically varies over the period of the amplitude modulation (milliseconds). We measured the acoustic radiation force on a steel sphere suspended in water and found that it agreed with the prediction of Eq. (1) within experimental error.[19]

B. Source transducer

Figure 1 illustrates the experiment depicting a gel sample containing a stainless steel sphere. Force is applied by the acoustic field of a circular, 19-mm-diameter, $f/4$, lead zirconate titanate (PZT) element that is transmitting sine-wave bursts at the resonant frequency of 1 MHz. Bursts 200 ms in duration were transmitted every 2 s to induce a maximum sphere displacement >20 μm for gels containing 3% w/w gelatin. The pressure field from the source transducer was measured in water using a recently calibrated

polyvanylidene fluoride (PVDF) membrane hydrophone (GEC-Research Ltd., Marconi Research Center, Chelmsford, UK). The results were used to estimate a primary radiation force at 60 μN.[19] The error on the force estimate was approximately 16% of the mean value and was determined primarily by the uncertainty in pressure estimates. The sphere was positioned on the beam axis at the 76-mm radius of curvature of the source. The location of the sphere was tracked in time by measuring and integrating the instantaneous sphere velocity.

C. Sphere velocity and displacement estimation

A Siemens Sono-line Antares system was used to estimate sphere velocity via pulsed-Doppler methods. A VF5-10 linear array transducer was driven by 1-cycle, 7.27-MHz voltage pulses to transmit nominally 2.5-cycle, 7-MHz acoustic pulses. Doppler-pulse transmission was repeated for a fixed beam-axis position on the time interval $T_s = 76.8$ μs. rf echo waveforms were sampled at 40 Msamples/s using the ultrasound research interface of the Antares system[20] and stored for offline processing. The axes of the source transducer and linear array intersected at the 1.5-mm-diameter steel sphere, and the beam axes were separated by $\theta = 30°$, as illustrated in Fig. 1.

The demodulated complex envelope $V[n, m']$ was computed for each Doppler echo waveform. The sample index $1 \leq n \leq N$ counts echo samples within an echo waveform in what is commonly referred to as "fast-time." The index $1 \leq m' \leq M'$ counts the waveforms in "slow-time."

We compute the lag-one correlation function estimate between adjacent pairs of echo waveforms using

$$\hat{\phi}[n, m] = V^*[n, 2m - 1]V[n, 2m], \quad m' = 2m - 1. \qquad (2)$$

The change in index from m' to $m (1 \leq m \leq M)$ avoids counting by 2. The estimate of instantaneous sphere velocity $\hat{v}_s$ from complex correlation estimates is[21,22]

$$\hat{v}_s[m] = \left(\frac{-c}{4 \pi f_c T_s \cos \theta} \right) \frac{1}{N_0} \sum_{n=n_0}^{n_0+N_0-1} \arg(\hat{\phi}[n, m]). \qquad (3)$$

c is the compressional-wave speed of sound in the gel medium (1.5 mm/μs), n_0 marks the first fast-time sample in the region of interest near the sphere-echo peak, N_0 is the number of fast-time samples in the region of interest, and arg($\cdot$) indicates the phase angle obtained from the arctangent of the ratio of imaginary to real parts of the argument. High-pass filtering in slow-time, which is frequently used in blood flow measurements (wall filter), was unnecessary because scattering from the gel was negligible compared to the sphere.

Finally, sphere displacement is estimated by integrating velocity estimates $\hat{x}(t) \equiv \int_0^t \hat{v}_s(t')dt'$, where $t' = 2mT_s$. Integration was performed numerically using a cumulative trapezoidal scheme.[23]

D. Hydrogel sample construction

Gelatin gel samples (250 bloom strength, type B, Rousselot, Buenos Aires, Argentina) were constructed to test acoustic radiation force measurements of shear modulus and viscosity. Gelatin powder and distilled water are heated in a water bath at a temperature between 65 and 68 °C for 1 h and periodically stirred. When the sample is cooled to 50 °C, 0.1% by weight formaldehyde is added and thoroughly mixed. Molten gelatin is poured into a cylindrical sample mold (diameter 7.5 cm, height 5.5 cm). Two or three stainless steel spheres 1.5 mm in diameter are widely dispersed within the cooling gel just prior to gelation. Samples with 3% or 4% w/w gelatin concentrations are homogeneous except for the isolated spheres that are separated by at least 1.5 cm.

Narrowband through-transmission measurements of compression-wave speed and attenuation coefficient[24] were made on samples without steel spheres and with 4% gelatin concentration. Measurements made at 21 °C in degassed water were first calibrated using a castor oil sample. Two phantoms were measured every 0.5 MHz between 7 and 12 MHz. The slope of the attenuation coefficient as a function of frequency was estimated to be 0.027 ± 0.003 dB mm^{-1} MHz^{-1}. Using no alcohol in the sample, the average speed of compressional waves was $c = 1506 \pm 0.34$ m s^{-1} over the frequency range of the measurement.

The material properties of the gelatin gels were verified independently through oscillatory rheometer experiments. Parallel plate shear experiments were conducted on an AR-G2 rheometer (TA Instruments, New Castle, DE). Circular specimens, 25 mm diameter and 2–4 mm high, were molded from the same gelatin used to make the large samples containing spheres. After 1 day of gelation, the specimens were removed from the molds and bonded to parallel plate fixtures using cyanoacrylate (Rawn America, Spooner, WI). 5% strain was applied over a frequency range from 0.1 to 10 Hz with ten sample points per decade of frequency. For both concentrations of gelatin, the measured storage modulus was averaged over the test range giving 321 ± 14 and 640 ± 17 Pa for 3% and 4% gelatin concentrations.

E. Modeling

The rheological behavior of hydrogels on a scale larger than the ultrasonic wavelength may be described as that of a continuum.[16] We propose to model the displacement $x(t)$ of a sphere embedded in gelatin as a simple harmonic oscillator,[25]

$$M_t \frac{d^2x(t)}{dt^2} + R \frac{dx(t)}{dt} + kx(t) = F(t). \qquad (4)$$

$F(t)$ is the driving force, M_t is the total mass on which the force acts, R is a damping constant related to the mechanical impedance of the gel (see Appendix), and k is an elastic constant. Because the uniaxial load is applied along the source transducer beam axis and movement of the sphere is in the same direction, x and F are the axial components of the corresponding vectors. For a step change in force over time from a constant value to zero, $F(t) = F_0(1 - \text{step}(t))$, the homogeneous solution for displacement obtained from Eq. (4) has the form

2930   J. Acoust. Soc. Am., Vol. 125, No. 5, May 2009

Orescanin *et al.*: Material property estimation

$$x(t) = \begin{cases} x_0, & t \leq 0 \\ Ae^{-\alpha t}\cos(\omega_d t + \varphi), & t > 0. \end{cases} \quad (5)$$

A is the displacement amplitude, $\alpha = R/2M_t$, $\omega_d = \sqrt{\omega_0^2 - \alpha^2}$ is the resonant frequency with damping, and $\omega_0 = \sqrt{k/M_t}$ is the resonant frequency without damping. From the initial conditions, $A = x_0/\cos\varphi$ and $\tan\varphi = -\alpha/\omega_d$.

It is important to include the surrounding gel in estimating the dynamic inertia of the system.[26] The total mass that reacts to the radiation force is $M_t = M_s + M_a$, where M_s is the mass of the sphere and $M_a = \frac{2}{3}\pi a^3 \rho_g$ is the added mass of surrounding gel, where a is the sphere radius and ρ_g is the density of the gel. The next step is to relate the constants k and R to rheological parameters μ and η.

The viscous drag force F_d experienced by a 1.5-mm sphere as it moves through incompressible and viscous gel at velocities <10 mm/s has a Reynolds number on the order of 0.02. Consequently Eq. (4) gives the linear approximation $F_d(t) = -Rv_s(t)$, and the classic Stokes equation for R is[27]

$$R = 6\pi a \eta, \quad (6)$$

where the parameter η has the SI units Pa s. In the Appendix, we show that R is the mechanical resistance or the real part of the impedance. This implies that η may be interpreted as the shear damping parameter, which within the frequency range of the experiments is defined as $\mu_2 + \mu_1 a/c_s$, where μ_2 is shear viscosity or the imaginary part of the complex shear modulus μ', μ_1 is the real part of the complex shear modulus μ', and c_s is the shear wave speed.

Ilinskii et al.[28] applied an analysis parallel to Stokes derivation to show that the elastic constant in the restoring force equation, $F_r(t) = -kx(t)$, is

$$k = 6\pi a \mu, \quad (7)$$

where μ, with the SI units Pa, approximates the shear elasticity, μ_1 (see Appendix for details).

Combining Eqs. (5)–(7) sphere displacement is modeled in terms of shear elasticity and shear damping parameter. The approach is to measure M_t and a independently and then numerically fit normalized displacement estimates $\hat{x}'(t) = \hat{x}(t)/\hat{x}_0$ to model values $x'(t) = x(t)/x_0$ obtained from Eqs. (5)–(7) with μ and η as free parameters. Normalization scales and shifts the response so that displacements have values between 0 and 1. Thus μ and η are estimated without knowledge of the applied force magnitude F_0.

III. RESULTS

We verified the proposed model and assumptions by conducting radiation force experiments. The 1-MHz source transducer transmitted 200-ms voltage bursts with the same amplitude in each experiment. Originally at rest, the sphere was suddenly displaced away from the transducer by the pulse a maximum distance x_0 (see Fig. 2) before being released to return to its original location. The imaging probe measuring the sphere velocity was transmitting and receiving Doppler pulses during the entire process.

The rf echo waveform in Fig. 3 shows that each Doppler pulse causes the steel sphere to ring. Because the echo
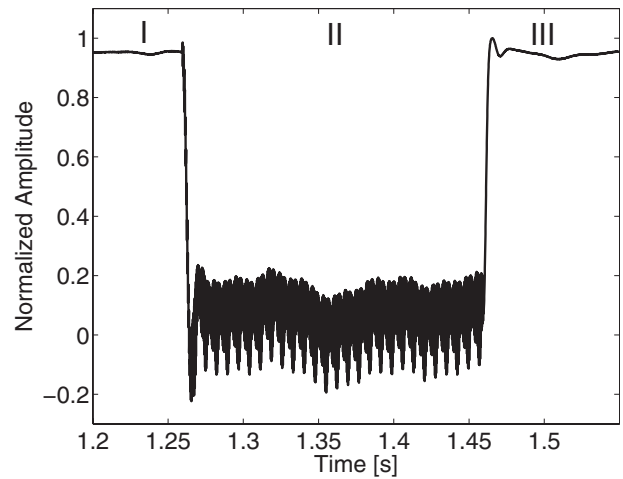
FIG. 2. Measurement of sphere displacement versus slow-time as determined from the change in Doppler echo phase. The sphere is embedded in a 3% gelatin gel. Region I is a time period before radiation force is applied and the sphere is at rest. Region II is a time period that the source transducer is transmitting a 1-MHz cw burst and the sphere is displaced away from the source. Oscillations indicate cross talk between the source and Doppler probes. Region III is the time period after the source is turned off and the sphere returns to its original position.

signal-to-noise ratio for tracking sphere velocity was very high, Doppler-pulse durations were set to 2.5 cycles to temporally resolve the first echo from subsequent ringing echoes. Echo phase is estimated near the peak of the first echo in Fig. 3.

From the data of Fig. 2, we can illustrate the process for a specific experiment. The spectral Doppler acquisition was initiated (region I). After approximately 1.26 s, the source transducer was turned on for 200 ms (region II). The phase of the Doppler echo from the sphere changed as the sphere was displaced by the acoustic force. On the time axis of the figure at 1.46 s, the source transducer is turned off [this time is set to $t = 0$ in Eq. (5)] and the sphere returns to the equilibrium position with the response of a slightly underdamped oscillator. We analyzed sphere displacement data as the
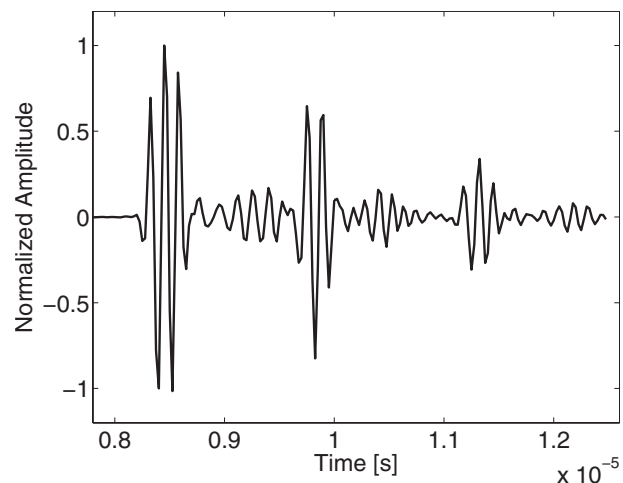
FIG. 3. Example of a broadband Doppler echo waveform versus fast-time. A single transmitted pulse is reflected from a steel sphere in 3% gelatin gel. Multiple echoes indicate ringing of the sphere.
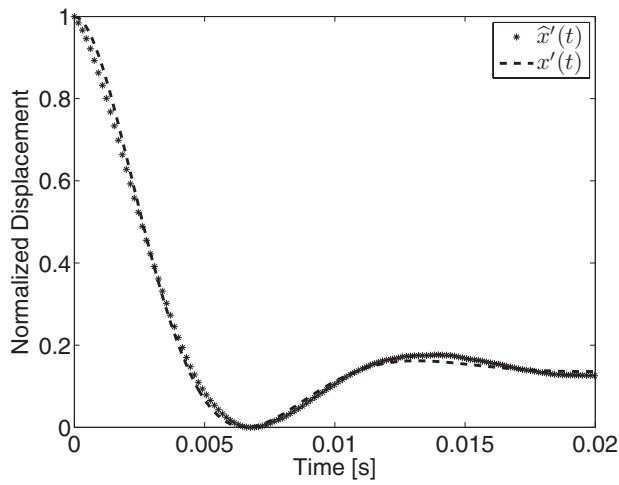
FIG. 4. Normalized sphere displacement measurements $\hat{x}'(t)$ from region III in Fig. 2 are compared with the model equation $x'(t)$ from Eq. (5). The minimum least-squares fit ($r^2 = 0.996$) was obtained for 3% gelatin gel aged 1 day to find $\mu = 317$ Pa and $\eta = 0.57$ Pa s.

source pulse was turned off rather than turned on to avoid cross talk between the source and Doppler probes as seen in Fig. 2, region II.

Figure 4 is an example of a comparison between a measured displacement time series $\hat{x}'[m]$ and samples from the best-fit model $x'[m]$ as a function of slow-time, $2mT_s$. For an M-point displacement time series with normally distributed random error, the material parameters μ and η are chosen to give the smallest residual sum of squares,[29]

$$r^2 = 1 - \frac{\sum_{m=1}^{M}(\hat{x}'[m] - x'[m])^2}{\sum_{m=1}^{M}(\hat{x}'[m] - \bar{x}')^2}, \quad \bar{x}' = \frac{1}{M}\sum_{m=1}^{M}\hat{x}'[m]. \quad (8)$$

r^2 is bounded from above by 1 (perfect agreement between data and model) and from below by zero, although it can be negative.

For small displacements, there is close agreement between measurements and the model, suggesting that gel deformation is linear as required by Eq. (5). Furthermore, if the normalized displacement is time invariant, then we may express the model as a linear system

$$x(t) = \int_{-\infty}^{\infty} dt\, h(t - t')(1 - \text{step}(t'))$$

with impulse response

$$h(t) = -\frac{dx}{dt} = Ae^{-\alpha t}(\alpha \cos(\omega_d t + \varphi) + \omega_d \sin(\omega_d t + \varphi)).$$

$$(9)$$

Equation (9) enables prediction of the displacement for any time-varying applied load for which the gel responds linearly.

Measurements of μ and η for 3% and 4% gelatin gels conducted over 4 days are presented in Figs. 5 and 6, respectively. Without adding a strong chemical cross linker, gelatin gels slowly increase their cross-link density, and thus gels continue to stiffen over days. Although gelatin gel responses are not strictly time invariant, the change in the impulse re-
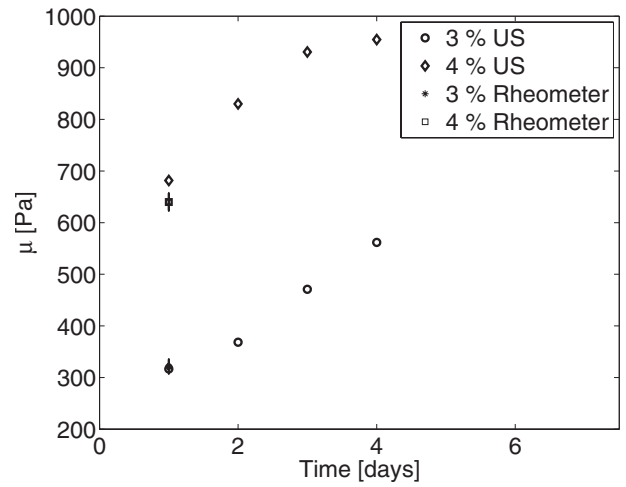
FIG. 5. Shear modulus as a function of gel age for 3% and 4% gelatin concentrations. Rheometer estimates of μ made on day 1 are also shown with error bars indicating ± 1 sd.

sponse is negligible over the duration of any experiment. Estimated values of the modulus and shear damping for gels with $C = 4\%$ gelatin concentration are larger than that at 3% for each day of the study. Gilsenan and Ross-Murphy[30] found that the shear modulus varies with the square of gelatin concentration, $\mu \propto C^2$, between 1% and 5%. Our data in Fig. 5 give a concentration dependence of $C^{2.7}$ on day 1 and $C^{2.4}$ on day 3.

As indicated in Fig. 5, rheometer measurements of the shear storage modulus were also made on day 1 for both gelatin concentrations. Five rheometer measurements were made on five different 3% gelatin samples to yield a mean and standard deviation of $\mu_r = 321 \pm 14$ Pa. The comparable radiation force estimate was 317 Pa. Three measurements were made on three different 4% samples to find $\mu_r = 640 \pm 17$ Pa. The comparable radiation force estimate is 681 Pa. Considering the rheometer measurements as a standard, radiation force estimates of shear modulus are accurate well within the observed day-to-day change in mean values. We were unable to obtain independent estimates of shear viscosity for the gels.
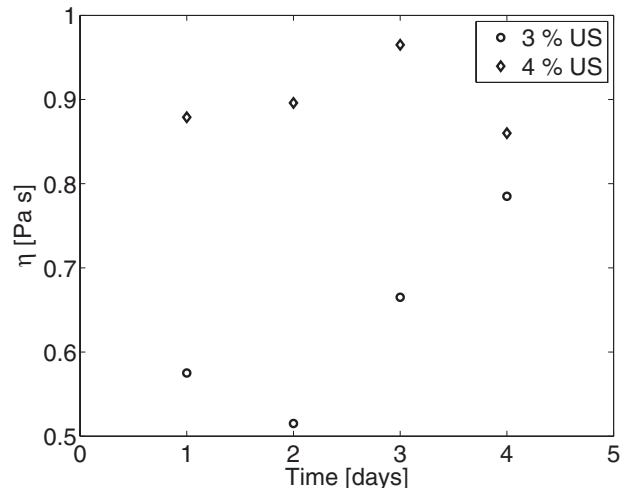
FIG. 6. Shear damping parameter as a function of gel age for 3% and 4% gelatin concentrations.

Radiation force measurements may also be used to estimate the shear speed c_s and shear viscosity μ_2; both are defined in the Appendix. At the end of the Appendix, we show that $\mu_1 \simeq \mu$, $\mu_2 = \eta - \mu_1 a/c_s$, and at low force frequencies where $\omega^2 \mu_2^2 \ll \mu_1^2$ we obtain the elastic result, $c_s \simeq \sqrt{\mu_1/\rho}$. Applying the 3% gelatin sample results at 24 h following gelation, $\mu = 317$ Pa and $\eta = 0.57$ Pa s, we estimate $c_s = 0.56$ m s^{-1} and $\mu_2 = 0.14$ Pa s. Our estimates are comparable to those reported by others using similar acoustic radiation force techniques.[31,32]

Intra-sample precision variability was estimated by measuring μ multiple times for a single sphere in one gelatin sample. The percent standard deviation was found to be approximately 3.5% of the mean, for example, $\mu = 317 \pm 11$ Pa. Boundary variability, i.e., proximity of each steel sphere to the gel sample surfaces, was examined by averaging μ measurements for different spheres placed in one gelatin sample. That standard deviation was approximately 7% of the mean. Inter-sample variability for μ was larger, 20% of the mean, primarily because of differences in gel preparation. The relatively small random experimental error is a consequence of the high echo signal-to-noise ratio.

IV. DISCUSSION

Mechanical parameter values are primary factors determining the ultrasonic sampling rate for pulsed-Doppler velocity estimation. Discussion near Eqs. (5)–(7) explains that the time-varying displacement amplitude, the frequency, and the phase are functions of μ and η. Estimation accuracy and precision will vary with the sampling rate depending on the bandwidth of the displacement spectrum. For linear gels, the displacement spectrum is the spectrum of the applied force filtered by the mechanical system response of the gel, $H(\omega; \mu, \eta)$. $H(\omega; \mu, \eta)$ is the temporal Fourier transform of Eq. (9) parametrized by the material properties.

The model spectrum of interest is the squared magnitude of the temporal Fourier transform of $x'(t)$ from Eq. (5). It has the Lorentz form

$$|X'(\omega)|^2 = \frac{1}{\alpha^2 + (\omega - \omega_d)^2}.$$

The 3-, 6-, and 20-dB bandwidths of the displacement spectrum are, respectively, $\Delta\omega = R/M_t$, $\sqrt{3}R/M_t$, and $\sqrt{99}R/M_t$. Therefore the upper limit on angular frequency is

$$\omega_{\max} = \omega_d + \Delta\omega/2 = \sqrt{\omega_0^2 - \alpha^2} + B\alpha, \tag{10}$$

where $B = 1$, $\sqrt{3}$, or $\sqrt{99}$ for the 3-, 6-, or 20-dB bandwidths.

To illustrate, Fig. 7 displays the displacement spectrum corresponding to the parameters for measurements on day 1 for 3% gelatin-concentration samples. The highest frequency in the 3-dB bandwidth is found from Eq. (10) to be $f_{\max} = \omega_{\max}/2\pi = 120$ Hz. The highest frequencies in the 6- and 20-dB bandwidths are 152 and 510 Hz, respectively.

The sampling theorem for bandlimited signals states that the minimum sampling rate needed to avoid aliasing is twice the value of the maximum frequency in the bandwidth. However, we must further increase the rate by the number of pulses in the velocity estimator ensemble, M_e. That is,
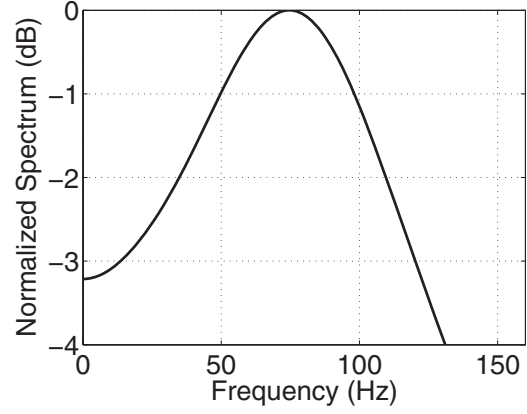
FIG. 7. Power spectrum of displacement for model parameters from 3% gelatin 24 h after gelation: $\mu = 317$ Pa and $\eta = 0.57$ Pa s. Characteristic parameters are the natural frequency $w_d/2\pi = 76.1$ Hz, half bandwidth $\Delta w/4\pi = 44$ Hz, and maximum frequency at the 3-dB limit $f_{\max} = 120.1$ Hz.

$$
\begin{aligned}
f_s &\gtrsim 2M_e f_{\max} \\
&= \frac{M_e}{\pi}(\sqrt{\omega_0^2 - \alpha^2} + B\alpha) \\
&= \frac{M_e}{\pi}\left(\sqrt{\frac{6\pi a\mu}{M_t} - \left(\frac{3\pi a\eta}{M_t}\right)^2} + \frac{3\pi Ba\eta}{M_t} \right).
\end{aligned}
\tag{11}
$$

For the experiments described in the previous paragraph, where we adopt the 6-dB bandwidth limit and $M_e = 2$, the pulse-repetition frequency (PRF $= f_s$) must exceed 608 Hz to avoid aliasing.

To decide on an acceptable lower bound on the sampling frequency, we oversampled the Doppler measurements at $f_s = 13$ kHz. We then incrementally downsampled this waveform sequence, being careful to apply the appropriate low-pass anti-aliasing filter as the Nyquist frequency changed, before processing. We thus obtained μ and η estimates as a function of f_s. We observed that a 15-dB bandwidth ($B = \sqrt{31}$) was sufficient to eliminate estimation errors within the intra-sample random error range of 7%. If the echo signal-to-noise ratio was reduced, for example, in stiff gels where sphere displacement is small or for low-scattering spheres, M_e could be increased to compensate as given by Eq. (11). There is also a tradeoff between time resolution for velocity estimates and distance to the target, in our case the sphere depth. Increasing f_s reduces the depth for the maximum unambiguous range to $c/2f_s$.[21]

We have evaluated Eq. (11) for a range of μ and η values estimated for gels and for the typical experimental parameters $M_e = 2$, $M_t = 14.7$ mg, and $B = \sqrt{31}$ (15-dB bandwidth). The corresponding minimum Doppler-pulse sampling rates are plotted in Fig. 8. It is important to point out that Eq. (11) is valid only for the Lorentz spectrum characteristic of the Kelvin–Voigt model, with total mass M_t as defined above. Changing the model to, for example, a three-element Zener model,[33] would require a new analysis to establish the minimum sampling frequency.

Quick estimates of μ and η may be made for a well-calibrated experimental system. If M_t and a are known, then η can be found directly from the 3-dB bandwidth of the step
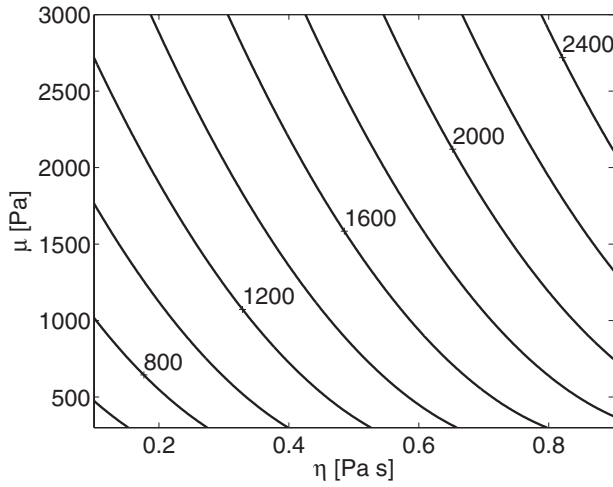
FIG. 8. Contour plot of the minimum sample frequency (i.e., PRF) in hertz from Eq. (11) as required to estimate μ and η as a function of these same material properties. We used a fixed ensemble size $M_e=2$, $B=\sqrt{31}$ (15-dB bandwidth), and $M_t=14.7$ mg. For example, for $\mu=1.5$ kPa and $\eta=0.5$ Pa s, $f_s \geq 1.6$ kHz.

response, $\eta=M_t \Delta \omega_{3\ dB}/6\pi a$. Applying this result and an estimate of the spectral peak to the expression for resonant frequency ω_d, we can estimate μ.

V. CONCLUSION

A damped harmonic oscillator model accurately predicts the movement of a hard sphere embedded in a congealed hydrogel to a sudden change in acoustic radiation force. This result suggests that the gel responds linearly to the force. We show how to relate parameters of the harmonic oscillator to the mechanical impedance of the system and material parameters. We estimated the coefficients of the complex shear modulus (shear elasticity and viscosity) with 7% intra-sample random experimental error by interpreting model parameters in terms of rheological elements. The radiation force estimates of modulus at two gel concentrations closely agree with independent measurements of the gels using a rheometer. This simple but accurate technique is designed to measure viscoelastic properties of 3D cell cultures remotely to maintain sterile conditions.

APPENDIX: MATERIAL PROPERTIES FROM MECHANICAL IMPEDANCE

The viscoelastic material properties of the gel medium surrounding a rigid sphere are frequently characterized by the mechanical impedance, Z, which relates, in three spatial dimensions, $\mathbf{y}=y_1, y_2, y_3$, and time, t, the resistance force of the sphere to motion, $\mathbf{F}(t,\mathbf{y})$, and the resulting sphere velocity, $\mathbf{v}_s(t,\mathbf{y})$, via the Ohm's law-like expression[34]

$$\mathbf{F}(t,\mathbf{y}) = -Z \times \mathbf{v}_s(t,\mathbf{y}). \tag{A1}$$

Force and velocity are vector quantities, impedance is a scalar, and all three are complex quantities in this expression. Stationary harmonic forces at radial frequency ω applied along the y_1 axis and of the form $F(t)=F_{\omega,1} \exp(-i\omega t)$ generate sphere velocities of the form $v_s(t)=v_{\omega,1} \exp(-i\omega t)$. In that situation, the material properties that influence Z are gel density $\rho \simeq 1$ g/cm^3, sphere radius $a=0.75$ mm, and the complex Lamè moduli $\mu'=\mu_1-i\omega\mu_2$ and $\lambda'=\lambda_1-i\omega\lambda_2$. μ_1 is shear elasticity, μ_2 is shear viscosity, λ_1 is volume compressibility, and λ_2 is volumetric viscosity. For the small forces used in our experiments, it is assumed that the gel responds linearly so the sphere velocity for an arbitrary time-varying force is a weighted linear superposition of velocities at each frequency in the force bandwidth. Further, it is assumed that the sphere is bound to the continuous, homogeneous, and isotropic gel.

Of course, the force and velocity vectors also vary spatially. For harmonic, compressional, plane waves traveling along the y_1 axis, $F(t,\mathbf{y})\hat{\mathbf{y}}_1=F_{\omega,1} \exp(ky_1-\omega t)$, the impedance is straightforward to find from Eq. (A1) and the one-dimensional wave equation, as shown in standard texts.[34]

The mechanical impedance Z for the case of an oscillating sphere was found by Oestreicher.[35] Making use of the spherical symmetry, he separately solved for the irrotational and incompressible components of the wave equation relating pressure and displacement in terms of spherical harmonics.[26] Integrating the pressure over the sphere to find force and for $v_s(t)=-i\omega x(t)$, he found

$$Z = -\frac{4}{3}\pi a^3 \rho i \omega \left\{ 1 - \left[\frac{1}{3}\left(1 - \frac{3(1-ik_c a)}{k_c^2 a^2} \right)^{-1} - \frac{2}{3}\left(1 - \frac{3(1-ik_s a)}{k_s^2 a^2} \right)^{-1} \right]^{-1} \right\}. \tag{A2}$$

The above expression is the form given by Norris [see Eq. (5) in Ref. 36]. In Eq. (A2), $k_c=(\rho\omega^2/(2\mu'+\lambda'))^{1/2}$ and $k_s=(\rho\omega^2/\mu')^{1/2}$ are, respectively, the compressional and shear complex wave numbers. The wave number $k_s=\omega/c_s+i\alpha_s$ may also be written as a function of the shear wave speed and shear wave attenuation constant, respectively,[37]

$$c_s = \omega/\Re\{k_s\} = \sqrt{\frac{2(\mu_1^2+\omega^2\mu_2^2)}{\rho(\mu_1+\sqrt{\mu_1^2+\omega^2\mu_2^2})}} \tag{A3}$$

and

$$\alpha_s = \Im\{k_s\} = \sqrt{\frac{\rho\omega^2(\sqrt{\mu_1^2+\omega^2\mu_2^2}-\mu_1)}{2(\mu_1^2+\omega^2\mu_2^2)}}. \tag{A4}$$

Oestreicher[35] commented that the number of constants in the Lamè moduli increases if time derivatives of order greater than 1 are required to model the data. For harmonic oscillations, the corresponding Lamè moduli will have added terms multiplied by increasing powers of $-i\omega$. Higher-order time derivatives generate frequency dependent Lamè moduli that appear experimentally as dispersion, i.e., frequency dependent wave speeds. It was shown experimentally[24] that gelatin is non-dispersive for compressional waves between 1
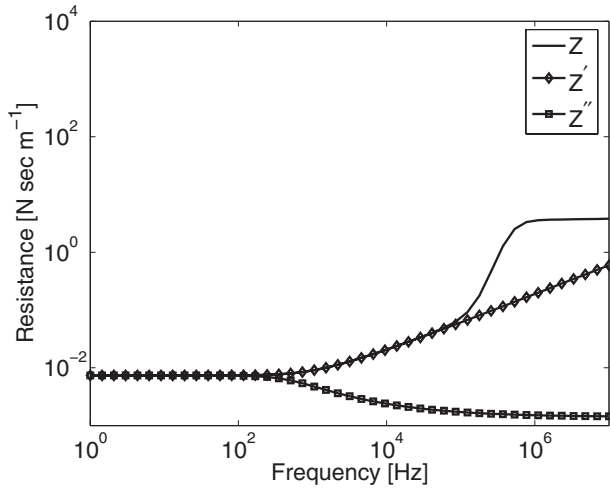
FIG. 9. Mechanical resistance (real part of impedance) for an oscillating sphere in 3% gelatin gel.
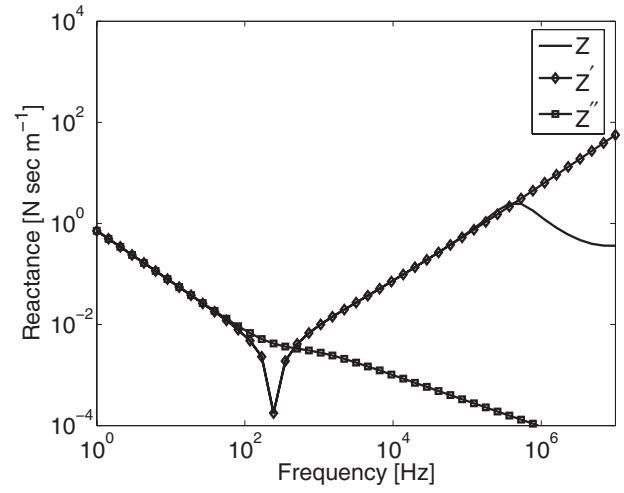
FIG. 10. Mechanical reactance (imaginary part of impedance) for an oscillating sphere in 3% gelatin gel.

and 10 MHz with and without particle scatterers. Applying Eq. (A3) and the values of μ_1 and μ_2 reported in Sec. III, it can be seen that c_s varies by less than 0.7% for clear gelatin gels at shear-wave frequencies less than 50 Hz. Consequently, it is reasonable to assume non-dispersive media for our low-frequency experiments.

In incompressible viscoelastic gels, the bulk modulus $\lambda + 2\mu/3$ becomes infinite while μ remains finite.[36] We measured $c_c = 1506$ m/s and $\mu_1 = 317$ Pa for clear 3% gelatin gels and adopt $\mu_2 = 0.1$ Pa s as Ilinskii et $al.$[28] Applying the expressions from the paragraph below Eq. (A2), we estimate that $c_s = 0.56$ m/s and $\lambda_1 = 2.25 \times 10^9$ Pa. Further, like Oestreicher,[35] we assume $\lambda_2 = 0$. Consequently, $k_c/k_s \ll 1$, and Eq. (A2) reduces to

$$Z' = -\frac{6\pi a \mu'}{i\omega}\left[\frac{k_s^2 a^2}{9} - (1 - ik_s a)\right]$$ (A5)

provided the sphere remains bound to the gelatin.[36] Expanding Eq. (A5) using $\mu' = \mu_1 - i\omega\mu_2$, we find

$$Z' = -6\pi a\left[\mu_2\left(1 - \frac{k_s^2 a^2}{9}\right) + \frac{\mu_1}{\omega}k_s a\right]$$
$$- i6\pi a\left[\frac{\mu_1}{\omega}\left(1 - \frac{k_s^2 a^2}{9}\right) - \mu_2 k_s a\right].$$ (A6)

Noting that $\mu_2/\mu_1 \ll 1$ and $a = 7.5 \times 10^{-4}$, we neglect all terms $\mathcal{O}(a^3)$ and $\mathcal{O}(\mu_2 a^2)$ to find

$$Z'' \simeq -6\pi a\left(\mu_2 + \frac{\mu_1 k_s a}{\omega} - i\frac{\mu_1}{\omega}\right).$$ (A7)

Finally, expanding k_s as a function of c_s and α_s we can rewrite Eq. (A7) as

$$Z'' = -6\pi a\left(\mu_2 + \frac{\mu a}{c_s} - i\frac{\mu_1}{\omega}(1 + \alpha_s a)\right).$$ (A8)

Impedance, Z, and its approximations, Z' and Z'', were evaluated numerically using values for constants listed above. The real parts are plotted in Fig. 9 and the imaginary parts in Fig. 10. There is no significant difference among the

three expressions provided $\omega/2\pi < 100$ Hz, where we are free to adopt Eq. (A8). The damping constant, R from Eq. (4), corresponds to the real part of the mechanical impedance, Z''. Comparing R in Eq. (6) with $\Re\{Z''\}$ in Eq. (A8), we find $\eta = \mu_2 + \mu_1 a/c_s$. Also, since $v_s(t) = -i\omega x(t)$, comparing μ from Eq. (7) with $\Im\{Z''\}$ in Eq. (A8) yields $\mu = \mu_1(1 + \alpha_s a) \simeq \mu_1$ for our experimental conditions.

[1] A. Itoh, E. Ueno, E. Tohno, H. Kamma, H. Takahashi, T. Shiina, M. Yamakawa, and T. Matsumur, "Breast disease: Clinical application of US elastography for diagnosis," Radiology **239**, 341–350 (2006).

[2] M. Fatemi and J. F. Greenleaf, "Ultrasound-stimulated vibro-acoustic spectrography," Science **280**, 82–85 (1998).

[3] E. A. Barannik, A. Girnyk, V. Tovstiak, A. I. Marusenko, S. Y. Emilianov, and A. P. Sarvazyan, "Doppler ultrasound detection of shear waves remotely induced in tissue phantoms and tissue in vitro," Ultrasonics **40**, 849–852 (2002).

[4] E. E. Konofagou and K. Hynynen, "Localized harmonic motion imaging: Theory, simulations and experiments," Ultrasound Med. Biol. **29**, 1405–1413 (2003).

[5] K. Nightingale, M. S. Soo, R. Nightingale, and G. Trahey, "Acoustic radiation force impulse imaging: In vivo demonstration of clinical feasibility," Ultrasound Med. Biol. **28**, 625–634 (2001).

[6] R. Sinkus, K. Siegmann, T. Xydeas, M. Tanter, C. Claussen, and M. Fink, "MR elastography of breast lesions: Understanding the solid/liquid duality can improve the specificity of contrast-enhanced MR mammography," Magn. Reson. Med. **58**, 1135–1144 (2007).

[7] Y. Qiu, M. Sridhar, J. K. Tsou, K. K. Lindfors, and M. F. Insana, "Ultrasonic viscoelasticity imaging of nonpalpable breast tumors: Preliminary results," Acad. Radiol. **15**, 1526–1533 (2008).

[8] D. E. Discher, P. Janmey, and Y. L. Wang, "Tissue cells feel and respond to the stiffness of their substrate," Science **310**, 1139–1143 (2005).

[9] T. A. Krouscop, P. S. Younes, S. Srinivasan, T. Wheeler, and J. Ophir, "Differences in the compressive stress-strain response of infiltrating ductal carcinomas with and without lobular features—Implications for mammography and elastography," Ultrason. Imaging **25**, 162–170 (2003).

[10] S. Kalyanam, R. D. Yapp, and M. F. Insana, "Poroviscoelastic behavior of gelatin hydrogels under compression: Implications for bioelasticity imaging," ASME J. Biomech. Eng. **131**, 1–21 (2009).

[11] M. Sridhar, J. Liu, and M. F. Insana, "Elasticity imaging of polymeric media," ASME J. Biomech. Eng. **129**, 259–272 (2007).

[12] M. Sridhar and M. F. Insana, "Ultrasonic measurements of breast viscoelasticity," Med. Phys. **34**, 4757–4767 (2007).

[13] R. D. Cardiff and N. Kenney, "Mouse mammary tumor biology: A short history," Adv. Cancer Res. **98**, 53–116 (2007).

[14] C. L. Shaffer, D. Hernando, J. Stastny, S. Kalyanam, J. Haldar, E. Chaney, X. Liang, and M. F. Insana, "Multimodality imaging development using

J. Acoust. Soc. Am., Vol. 125, No. 5, May 2009

Orescanin *et al.*: Material property estimation   2935

3-D gel cultures," in BMES Annual Fall Conference, Los Angeles CA (2007), p. 374.

[15]J. Xu, R. Kong, R. Bhargava, and M. F. Insana, "3-D cell co-cultures to develop multimodality breast imaging," in BMES Annual Fall Conference, St. Louis, MO (October 2008).

[16]J. D. Ferry, *Viscoelastic Properties of Polymers*, 3rd ed. (Wiley, New York, 1980).

[17]B. Fabry, G. N. Maksym, J. P. Butler, M. Glogauer, D. Navajas, N. A. Taback, E. J. Millet, and J. J. Freedberg, "Time scale and other invariants of integrative mechanical behavior in living cells," Phys. Rev. E **68**, 041914 (2003).

[18]T. Hasegawa and K. Yosioka, "Acoustic-radiation force on a solid elastic sphere," J. Acoust. Soc. Am. **46**, 1139–1143 (1969).

[19]M. Orescanin and M. F. Insana, "Ultrasonic radiation forces for elasticity imaging of 3-D tissue models," Proc. SPIE **6513**, OH1–OH11 (2007).

[20]S. S. Brunke, M. F. Insana, J. J. Dahl, C. Hansen, M. Ashfaq, and H. Ermert, "An ultrasound research interface for a clinical system," IEEE Trans. Ultrason. Ferroelectr. Freq. Control **54**, 198–210 (2007).

[21]J. A. Jensen, *Estimation of Blood Velocities Using Ultrasound: A Signal Processing Approach* (Cambridge University Press, New York, 1996).

[22]R. J. Doviak and D. S. Zrnic, *Doppler Radar and Weather Observations*, 3rd ed. (Academic, San Diego, 1993).

[23]A. W. Al-Khafaji and J. R. Tooley, *Numerical Methods in Engineering Practice* (Oxford University Press, Oxford, 1985).

[24]E. L. Madsen, J. A. Zagzebski, and G. R. Frank, "Oil-in-gelatin dispersions for use as ultrasonically tissue-mimicking materials," Ultrasound Med. Biol. **8**, 277–287 (1982).

[25]We propose a simple engineering model for which two parameters μ and η may be found. To interpret these parameters as physical quantities, we outline in the Appendix a classic physical model from the literature, and we give the conditions where the parameters may be interpreted as material properties.

[26]S. H. Lamb, *Hydrodynamics*, 6th ed. (Cambridge University Press, Cambridge, UK, 1932).

[27]P. Kundu, I. M. Cohen, and H. H. Hu, *Fluid Mechanics* (Academic, New York, 2004).

[28]Y. A. Ilinskii, G. D. Meegan, E. A. Zabolotskaya, and S. Y. Emilianov, "Gas bubble and solid sphere motion in elastic media in response to acoustic radiation force," J. Acoust. Soc. Am. **117**, 2338–2346 (2005).

[29]A. C. Cameron and F. A. G. Windmeijer, "R-squared measures for count regression models with applications to health-care utilization," J. Bus. Econ. Stat. **14**, 209–220 (1996).

[30]P. M. Gilsenan and S. B. Ross-Murphy, "Shear creep of gelatin gels from mammalian and piscine collagens," Int. J. Biol. Macromol. **29**, 53–61 (2001).

[31]J. Bercoff, M. Tanter, M. Muller, and M. Fink, "The role of viscosity in the impulse diffraction field of elastic waves induced by the acoustic radiation force," IEEE Trans. Ultrason. Ferroelectr. Freq. Control **51**, 1523–1536 (2004).

[32]S. Chen, M. Fatemi, and J. F. Greenleaf, "Remote measurement of material properties from radiation force induced vibration of an embedded sphere," J. Acoust. Soc. Am. **112**, 884–889 (2002).

[33]M. Ahearne, Y. Yang, A. J. El Haj, K. Y. Then, and K. K. Liu, "Characterizing the viscoelastic properties of thin hydrogel-based constructs for tissue engineering applications," J. R. Soc., Interface **2**, 455–463 (2005).

[34]L. E. Kinsler, A. R. Frey, A. B. Coppens, and J. V. Sanders, *Fundamentals of Acoustic*, 4th ed. (Wiley, New York, 2000).

[35]H. L. Oestreicher, "Field and impedance of an oscillating sphere in a viscoelastic medium with an application to biophysics," J. Acoust. Soc. Am. **23**, 707–714 (1951).

[36]A. N. Norris, "Impedance of a sphere oscillating in an elastic medium with and without a slip," J. Acoust. Soc. Am. **119**, 2062–2066 (2006).

[37]E. L. Madsen, H. J. Sathoff, and J. A. Zagzebski, "Ultrasonic shear wave properties of soft tissues and tissuelike materials," J. Acoust. Soc. Am. **74**, 1346–1355 (1983).